2011 American Control Conference
on O'Farrell Street, San Francisco, CA, USA
June 29 - July 01, 2011

An Energy Efficient Pneumatic-electrical System and Control Strategy Development

Xing Luo, Hao Sun and Jihong Wang, *Senior Member, IEEE*

Abstract— **Pneumatic actuators are widely used in industry and many other applications, whereas low energy efficiency has been recognized as a critical drawback compared with corresponding hydraulic and electrical actuators. The paper presents a new hybrid pneumatic-electrical system aiming at energy efficiency improvement by recovering exhaust air energy from pneumatic actuator outlets to generate electricity. A closed-loop control strategy is proved to be essential to ensure the exhaust energy recovery work properly and to maintain existed actuator operations simultaneously. The whole system mathematical model and the simulation results are presented in the paper. The laboratory test results are also given. The simulation and experimental study demonstrate that the designed system with the proposed control strategy can operate at the relative higher energy efficiency state for the specified working conditions.**

I. Introduction

COMPRESSED air has been widely used in many fields, especially in industry to generate driving forces. From the statistics of the U.S. Department of Energy's Office of Energy Efficiency and Renewable Energy, air compressors consume as much as 20% of all electricity usage in industrial plants [1]. In the UK, over 10% of the National Grid output is used to generate compressed air in industry [2]. Compared with hydraulic and electrical counterparts, pneumatic actuating systems have some distinct advantages, such as low cost, mechanical simplicity. However, the significant weakness of pneumatic actuators is low energy efficiency. British Fluid Power Association reported that, normally only 23%-30% energy efficiency is achieved for pneumatic systems, against 80% for electrical systems and 40% for hydraulic systems [3]. The main reason for low efficiency is the open-circuit structure of the air flow in pneumatic systems ([4] [5]).

For efficiency improvement, a straightforward thinking would naturally come from closing or modifying the air flow circuit at the discharging port for exhaust energy recovery. This will require a device connecting to the down-stream with high energy efficiency. The relative new scroll-type air motor technology bring the possibility for this proposition due to its high energy efficiency ([5][6]), which inherited from its corresponding machinery, the scroll compressor [7]. Meanwhile, as the modification of the down-stream air circuit will affect the up-stream actuator's operation, a suitable control strategy is indispensable to the whole system.

The proposed system structure is illustrated in Fig. 1. The system can be considered to have three parts. (1) Up-stream subsystem: it serves as a simulation for real industrial situations to generate exhaust air. It includes the air supply, pneumatic actuators and the main load. (2) Down-stream subsystem: it is composed of an intermediate air tank, a scroll-type air motor, an AC generator and its electric load. The purpose of using an air tank is for buffering the down-stream negative effects to the up-stream. The exhaust energy is recycled by the scroll air motor. (3) Controller: an appropriate controller is employed for supporting the whole system operation. The paper starts from presenting the system mathematical model and then simulation studies. The test system is described and the experimental results are presented.

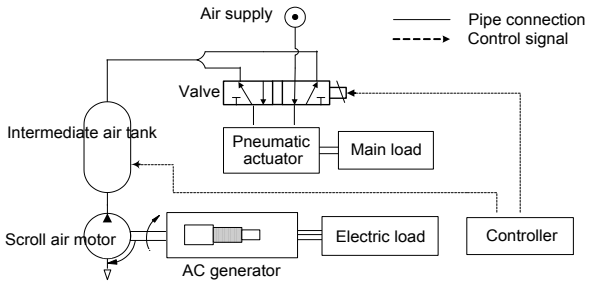

Fig. 1 Block diagram of the pneumatic-electricity system

II. Description of Mathematical Model of the System

A. Mathematical model for pneumatic cylinders

The coordinate system of a typical double acting rodless cylinder is illustrated in Fig. 2. The actuator can be controlled by using two three-port valves or single five-port valve. The mathematical model can be described by ([8]),

$$\dot{x}_1 = x_2 \tag{1}$$

$$\dot{x}_2 = \frac{1}{m_{cylinder}}\left[-K_{fc}x_2 - K_{S-C}S(x_2,x_3,x_4) + A_{c\_a}x_3 - A_{c\_b}x_4\right] \tag{2}$$

$$\dot{x}_3 = \frac{k}{(l/2+x_1+\Delta)}\left[-x_3x_2 + \frac{RT_s}{A_{c\_a}}c_d c_0 w_{c\_a}u_1\hat{f}(x_3,P_s,P_e)\right] \tag{3}$$

$$\dot{x}_4 = \frac{k}{(l/2-x_1+\Delta)}\left[x_4x_2 + \frac{RT_s}{A_{c\_b}}c_d c_0 w_{c\_b}u_2\hat{f}(x_4,P_s,P_e)\right] \tag{4}$$

This work was supported in part by the Joule's Center from the Northwest Development Agent, U.K., in part by the Engineering and Physical Sciences Research Council under Grant EP/F027265/1, in part by the Advantage West Midlands and the European Regional Development Agency for the support of Birmingham Science City Energy Efficiency and Demand project, and in part by China 863 programme (2009AA05Z212).

X. Luo, H. Sun and J. Wang are with the School of Engineering, University of Warwick, Coventry, CV4 7AL, U.K. (Corresponding author: Prof. J Wang, E-mail:Jihong.Wang@warwick.ac.uk).

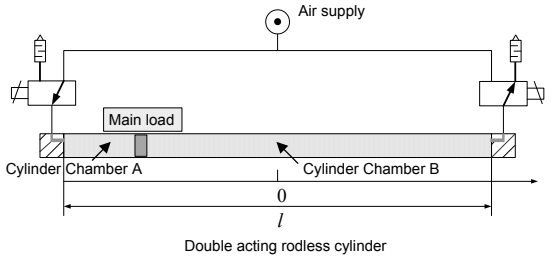

Fig. 2 Coordinate system of a pneumatic system

where x_1 represents the piston position, x_2 is the piston velocity, x_3, x_4 are the pressures of the two chambers, u_1, u_2 are the spool valve opening positions, the subscripts c_a, c_b are for cylinder inlet and outlet chambers individually, A is ram area, C_d is discharge coefficient, C_0 is the flow constant, Δ is the generalized residual chamber volume, K_{fc} is the cylinder viscous frictional coefficient, k is the specific heat constant, l is stroke length, w represents the mass flow rate, $m_{cylinder}$ is cylinder payload, P_s, P_e stand for supply pressure and exhaust pressure respectively, R is universal gas constant, T_s is the supply pressure. The values of constants appear in the model (k, C_0, C_d, R, C_r, C_k), and the function formulas of $\hat{f}(\cdot)$ and $K_{S-C}S(\cdot)$ are given in [8].

B. Mathematical model of a vane-type air motor

A vane-type air motor with eight vanes is schematically shown in Fig. 3. Its working principle is: when the rotor is rotating, the vanes tend to slide outward as the centrifugal force and divide the air motor control volume into two chambers – driving and driven chambers; the force by compressed air drives the rotor rotating in either clockwise or anticlockwise direction. The mathematical model of the vane-type air motor is described as follows ([9]):

$$\dot{x}_5 = x_6 \tag{5}$$

$$\dot{x}_6 = \frac{L_v}{2J_V}(x_7 - x_8)\times(e^2\cos 2x_5 + 2eB\cos x_5 + B^2 - r_v^{\,2}) - \frac{K_{cv}}{J_V}S_v(x_6) - \frac{K_{fv}}{J_V}x_6 \tag{6}$$

$$\dot{x}_7 = \frac{kRT_sC_dC_0D_{v\_a}u_3 f(x_7,P_s,P_e)}{V_{v\_a}x_5} - \frac{k}{V_{v\_a}x_5} + \frac{dV_{v\_a}x_5}{dx_5}x_7x_6 \tag{7}$$

$$\dot{x}_8 = \frac{kRT_sC_dC_0D_{v\_b}u_4 f(x_8,P_s,P_e)}{V_{v\_b}x_5} - \frac{k}{V_{v\_b}x_5} + \frac{dV_{v\_b}x_5}{dx_5}x_6x_8 \tag{8}$$

where x_5 is the motor rotor position, x_6 represents the motor rotor speed, x_7, x_8 are the pressures of two chambers of the vane-type air motor, u_3 and u_4 are the spool valve opening positions, the subscripts v_a, v_b are for Vane Chamber A and Chamber B individually, D is effective port width of the control valve, B is the radius of air motor body, e is motor eccentricity. r_v is motor rotor radius, L_v is vane active length in the axial direction, K_{fv} and K_{cv} are the vane-type of air motor dynamic and static frictional coefficients, P_s, P_e stand for supply pressure and exhaust pressure respectively. V is the control volume inside the vane chambers. J_v is the motor inertia. The function of $f(\cdot)$ is shown in [9], and $S_v(\cdot)$ is:

$$S_v(x_6) = \begin{cases} 1, & x_6 = 0 \\ sign(x_6)\partial_c \quad (0 \le \partial_c < 1) & x_6 \ne 0 \end{cases} \tag{9}$$

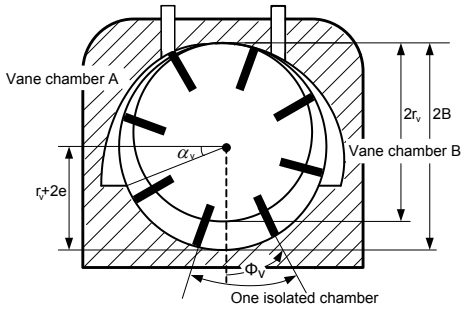

Fig. 3 Structure of a vane-type air motor with eight vanes

C. Mathematical model of a scroll-type air motor

The scroll-type air motor is a key component for the proposed system, and its high energy efficiency characteristic is resulted from its smart mechanical structure (for details, refer to [6] [10]). A scroll-type air motor working process includes three phases, charging, expansion, and discharging phase, which are associated with three different types of chambers, i.e., the central, the side and the exhaust chambers [10]. During the air motor operation, the compressed air energy in chambers forces and pushes the moving scroll wobbles in the direction to drive the crank.

From analyzing the scroll geometry and applying the thermodynamic theory, a complete thermodynamic model of the scroll-type air motor can be described by ([5] [10]),

$$\dot{T}_{s\_c} = \frac{\frac{\dot{m}_{in}h_{in}}{V_{s\_c}} - \frac{\dot{V}_{s\_c}}{V_{s\_c}}[X_{air}]\hat{h}_{s\_c} - [\dot{X}_{air}]\hat{h}_{s\_c} + P_{s\_c}[\dot{X}_{air}]/[X_{air}]}{[X_{air}]C_{p,air}(T_{s\_c}) - P_{s\_c}/T_{s\_c}} \tag{10}$$

$$\dot{P}_{s\_c} = \frac{1}{V_{s\_c}}\left(\frac{\dot{m}_{s\_c}}{M_{air}}RT_{s\_c} + R\dot{T}_{s\_c}\frac{m_{s\_c}}{M_{air}} - P_{s\_c}\dot{V}_{s\_c}\right) \tag{11}$$

$$\dot{T}_{s\_s} = \frac{-(\dot{V}_{s\_s}/V_{s\_s})([X_{air}]\hat{h}_{s\_s}) - [\dot{X}_{air}]\hat{h}_{s\_s} + P_{s\_s}[\dot{X}_{air}]/[X_{air}]}{[X_{air}]C_{p,air}(T_{s\_s}) - P_{s\_s}/T_{s\_s}} \tag{12}$$

$$\dot{P}_{s\_s} = \frac{1}{V_{s\_s}}\left(R\dot{T}_{s\_s}\frac{m_{s\_s}}{M_{air}} - P_{s\_s}\dot{V}_{s\_s}\right) \tag{13}$$

$$\dot{T}_{s\_e} = \frac{-\frac{\dot{m}_{out}h_{s\_e}}{V_{s\_e}} - \frac{\dot{V}_{s\_e}}{V_{s\_e}}([X_{air}]\hat{h}_{s\_e}) - [\dot{X}_{air}]\hat{h}_{s\_e} + P_{s\_e}\frac{[\dot{X}_{air}]}{[X_{air}]}}{[X_{air}]C_{p,air}(T_{s\_e}) - P_{s\_e}/T_{s\_e}} \tag{14}$$

$$\dot{P}_{s\_e} = \frac{1}{V_{s\_e}}\left(\frac{\dot{m}_{s\_e}}{M_{air}}RT_{s\_e} + R\dot{T}_{s\_e}\frac{m_{s\_e}}{M_{air}} - P_{s\_e}\dot{V}_{s\_e}\right) \tag{15}$$

$$\dot{\omega}_{scroll} = \sum_{n=0,1,2,\ldots}\frac{1}{J_s}[-K_{fs}\omega_{scroll} + zr_s\hat{P}(2\rho_0 + 2\gamma\alpha_s + (4n_s+1)\gamma\pi)] \tag{16}$$

where the subscripts s_c, s_s, s_e represent for the scroll central, side and exhaust chambers individually. The subscripts in, out represent air in and out respectively. $[X_{air}]$ is the molar volumetric concentration of air. M is the molar mass of air. $\hat{h}$ is the specific enthalpy of air on a molar basis.

$C_{p,air}(T)$ is the specific heat of the air per mole at the temperature T . P is the air pressure. T stands for temperature. V represents volume. $\dot{m}$ is mass flow rate. h refers to the air enthalpy. ω_{scroll} is the scroll rotor angular speed. J_s is the inertia of the scroll, and K_{fs} is the coefficient of the kinematic friction. z is the depth of the scrolls. ρ_0 is the initial radius of the curvature for the scroll curve. γ is the slope of the radius of curvature. r_s is the radius of the orbit of the moving scroll motion. α_s is the scroll orbit angle. n_s is the number of the scroll wrap.

D. Mathematical model of a AC generator

A permanent magnet synchronous generator (PMSG) has been chosen for the test system as it is simple in structure. The mathematical model of PMSG is described below [11]:

$$\dot{\omega}_G = \frac{1}{J_G}(T_G - T_e - F_G\omega_G) \tag{17}$$

$$\dot{\theta}_G = \omega_G \tag{18}$$

$$\dot{i}_d = \frac{1}{L_d}v_d - \frac{R_G}{L_d}i_d + \frac{L_q}{L_d}p_G\omega_G i_q \tag{19}$$

$$\dot{i}_q = \frac{1}{L_q}v_q - \frac{R_G}{L_q}i_q - \frac{L_d}{L_q}p_G\omega_G i_d - \frac{\lambda\, p_G\omega_G}{L_q} \tag{20}$$

$$T_e = \frac{3}{2}p_G[\lambda\, i_q + (L_d - L_q)i_d i_q] \tag{21}$$

$$v_q = \frac{1}{3}[\cos(p_G\theta_G)\times(2v_{ab} + v_{bc}) + \sqrt{3}v_{bc}\sin(p_G\theta_G)] \tag{22}$$

$$v_d = \frac{1}{3}[\sin(p_G\theta_G)\times(2v_{ab} + v_{bc}) + (-\sqrt{3}v_{bc}\cos(p_G\theta_G))] \tag{23}$$

where the subscripts a,b,c,d,q mean the a,b,c,d,q axis respectively. ω_G is angular velocity of the generator rotor. θ_G is the generator rotor angle position. J_G is the inertia of the generator. T_G and T_e stand for the generator drive torque and electromagnetic torque. F_G is combined viscous friction of the generator rotor and its load. R_G is resistance of the stator windings. L_q, L_d are the resulted q and d axis inductances individually. i and v are current and voltage in the different axes. p_G is the number of pole pairs in the generator. λ is the amplitude of the flux induced by the permanent magnets of the rotor. The Park's transformation is employed for transforming X_{abc} (3 phase coordinates) to X_{dq} (DQ rotating coordinates).

Integrating all the equations for different parts of the system, the whole system model can be derived. Due to the limitation of pages for the paper, it is impossible to give the detailed description for the mathematical model of each subsystem. They can be found in the reference list of the paper ([5][8][9][10][11]).

III. CONTROL STRATEGY STUDY

The model derived in Section II was implemented in the Matlab/Simulink environment. Fig. 4 and Fig.5 show dynamic responses of a pneumatic cylinder and an air motor connecting with the down-stream energy recovery system respectively without applying any control. The simulation was conducted by engaging the scroll air motor at 1.5seconds after the up-stream pneumatic actuators have been in operation. It is seen that the exhaust pressures of the up-stream subsystem increase and the speeds of the pneumatic actuators decrease. Therefore, the working conditions of the up-stream are varied due to connecting with the down-stream scroll air motor.

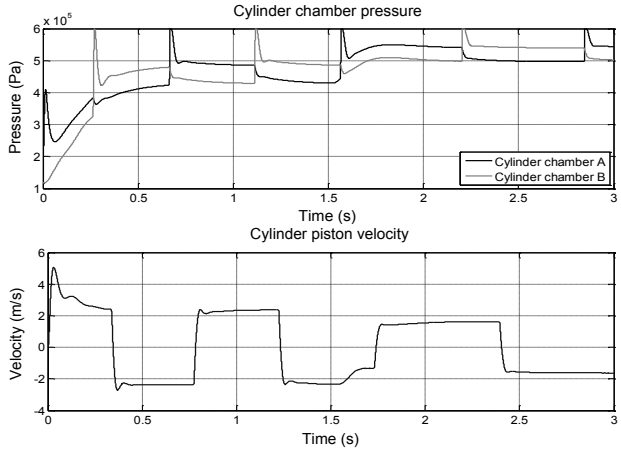

Fig. 4 Dynamic response of the non-controlled energy recovery system (connecting to a cylinder exhaust)

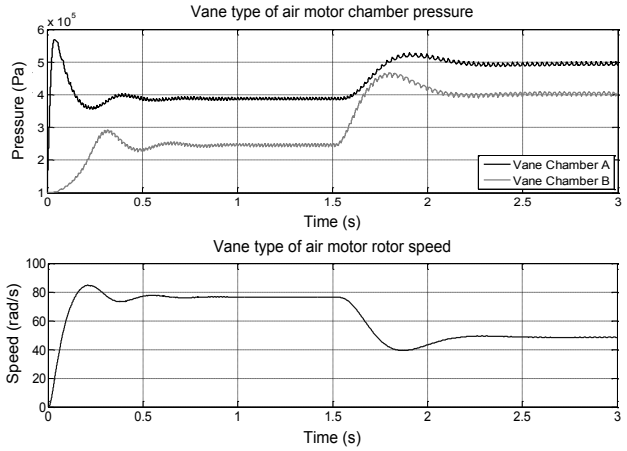

Fig. 5 Dynamic response of the non-controlled energy recovery system (connecting to a vane-type motor exhaust)

Based on the above simulation study, a closed-loop control must be introduced to the designed system. It need manage the overall system to maintain the up-stream actuator operation status and to ensure the down-stream scroll recycling work at the same time. A combination of a PID and an on/off control is employed to the system as shown in Fig.6. Two controllers are used: one on/off controller associated with an on/off valve is to keep the pressure inside of the intermediate air tank at a certain level; one PID controller imposed onto a proportional valve is to regulate the whole system air flow and to keep the speeds of the up-stream actuators' motion.

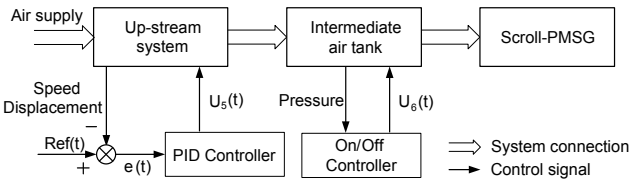

Fig. 6 Schematic of the control system

Fig. 7 shows the simulation results of dynamic responses of the controlled energy recovery system connecting with a pneumatic cylinder, which include the cylinder piston velocity and piston position variation histories. The simulation was conducted by engaging the down-stream scroll air motor at 1.5 seconds after the up-stream cylinder has been in operation. It can be seen that the cylinder piston movement can be maintained at near to the desired level. The limitations for the pressures of the intermediate air tank are set to be at $P_{\max} = 3.1\times10^5\,Pa$ and $P_{\min} = 2.8\times10^5\,Pa$, i.e., when the tank pressure is higher than $3.1\times10^5\,Pa$, the on/off valve for the tank is fully open to release the air; when the pressure is lower than $2.9\times10^5\,Pa$, the valve is completely closed.

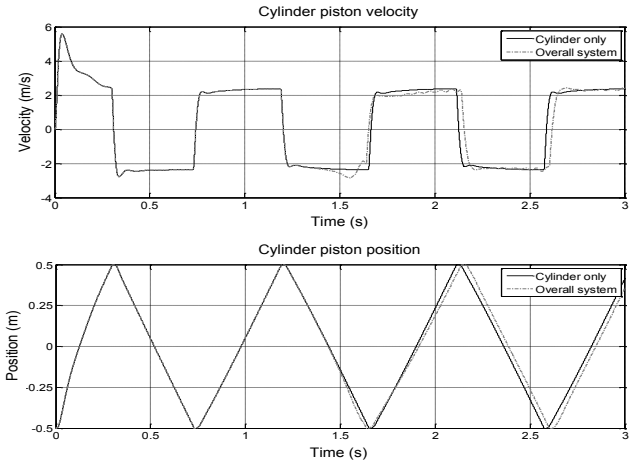

Fig. 7 Dynamic response of the overall system with controllers connected (Connecting to a cylinder exhaust)

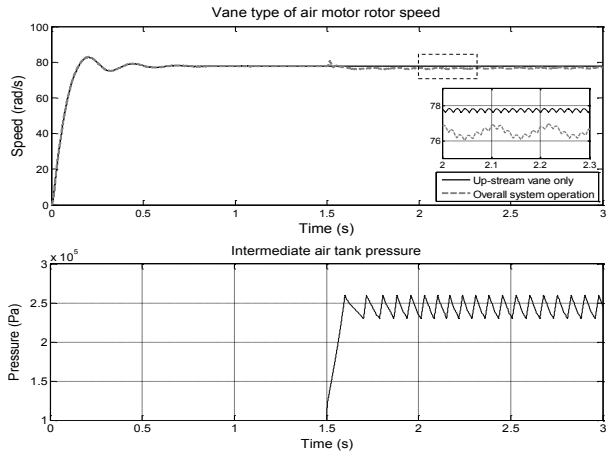

Fig. 8 Dynamic response of the overall system with controllers connected (Connecting to a vane-type air motor exhaust)

Accordingly, the simulation results of dynamic responses of the controlled overall system for recycling the vane-type air motor exhaust energy are shown in Fig. 8. The vane-type air motor rotation angles and the rotating speeds in two situations were presented respectively, i.e., with and without engaging the recycling mechanism. From Fig. 8, it is shown that the pressures of the intermediate air tank are limited to have the range of $P_{\max} = 2.6\times10^5\,Pa$ and $P_{\min} = 2.3\times10^5\,Pa$. Therefore, with the controllers for the two valves in action, the up-stream movement can be maintained and the down-stream recycling system is also in operation. And the whole system energy efficiency will be initially analyzed in the last section of the paper.

IV. Experimental Tests

The overall system test rig is set up in the authors' research laboratory to implement the whole process from a vane-type air motor actuator to the exhaust air recycling mechanism, which is shown in Fig. 9. A dSPACE real-time controller card (Model: RTI1104) is employed for collecting the experimental data from sensors and controlling the system valves. The test rig includes a vane-type air motor, a scroll-type air motor, a permanent magnet synchronous generator and its 3-phase electric load, an intermediate air tank, a DC generator and its electric load as the main load for the vane type air motor, pneumatic valves, pressure and flow measurements, a velocity sensor, etc. The proportional valve is used to control the compressed air input to the whole system. The on/off valve uses to control the intermediate air tank pressure.

The scroll-type air motor model has been validated (the scroll-type air motor had been modified from a scroll compressor, refer to [10]). And the vane-type air motor model was also validated in the same way. The majority parameters of the DC generator and the PMSG are available in the associated handbooks ([12] [13]). The unknown parameters for models can be identified using intelligent optimization algorithms together with the laboratory experimental data (refer to [14]).

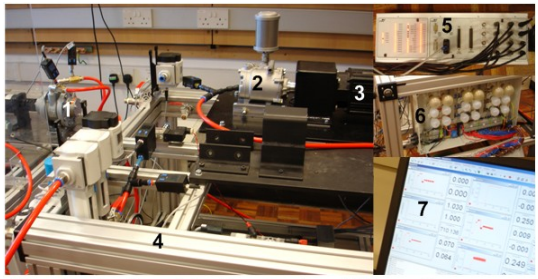

1-Vane type air motor 2-Scroll type air motor 3-AC generator
4-Intermediate air tank 5-dSPACE Controller connection interface
6-Lamp panel 7-Data acquisition/Controller monitoring interface

Fig. 9 The picture for the pneumatic-electrical system test rig

Fig. 10 shows the experimental results of the pneumatic-electricity system for exhaust energy recovery without interaction controllers. The real-time sampling rate is set to be 0.01s. The pressure from the air supply is about $6.5\times10^5\,Pa$.

The 3-phase electric load for the PMSG uses a lamp panel, two lamps 110V/60W in each phase. The recycling mechanism is engaged at the time of 19 seconds after the test starts. From Fig. 11, it can be seen that, when the up-stream is connected to the down-stream, the air motor exhaust pressure increases and the motor rotor speed drops.

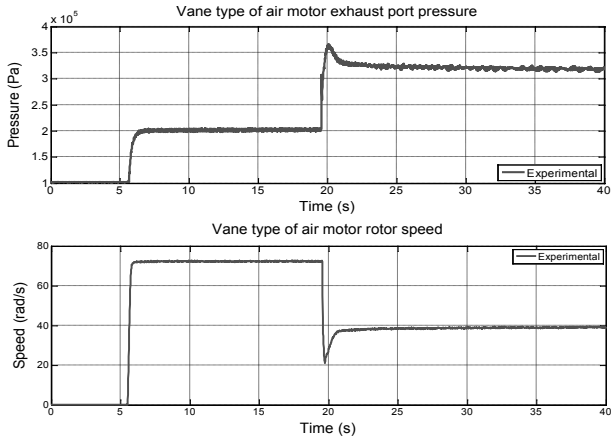

Fig. 10 Experimental results of the non-controlled energy recovery system

Fig. 11 shows the experimental results of the controlled pneumatic-electrical system, which include the control signal of the on/off valve, the vane-type air motor rotor speed and the scroll-type air motor intake pressure. The system sampling time sets at 0.01s. The pressure from the air supply is set to be $5.6\times10^5\,Pa$. The 3-phase electric load for the PMSG still uses the lamp panel mentioned above. The recycling system is activated at the 13th second when the up-stream vane-type air motor starts its operation. The pressure of the air tank is limited within the range of $P_{\max}=2.6\times10^5\,Pa$ and $P_{\min}=2.3\times10^5\,Pa$. From Fig. 11, the scroll-type air motor intake pressure has a slight oscillation due to the on/off valve operation. Also it is noticed that the speed of the up-stream actuator is less smooth than the speed while no recovering mechanism is involved. This can be improved by applying a strengthened speed controller which considers as one of the tasks in the next stage of the research work. Through repeated experimental tests, the overall test system can work well in a certain range depended on the reasonable settings of the pressure limits of air tank.

V. Energy Efficiency Analysis

According to the complete system shown in Fig.1, the energy transmission and conversion is schematically shown in Fig.12. The up-stream actuator system converts the energy carried by the compressed air to mechanical kinetic energy and then to drive the main load. The exhaust air energy flows into the scroll-type air motor through the intermediate air tank. Finally, the scroll-type air motor in turn drives the PMSG and its electric load. For such an energy conversion and transmission process, energy losses are inevitable, such as pneumatic actuator operation losses in both the up-stream and the down-stream including the friction loss, the leakage loss, etc. Energy efficiency can be analysed by calculating the ratio between the useful output power and the whole system employed air power ([10][18]).

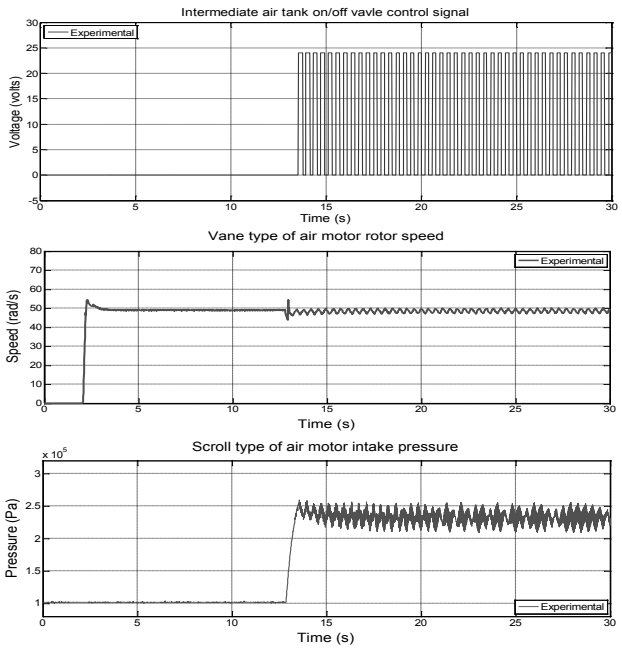

Fig. 11 Experimental results of the overall system with controllers (recycling energy from a vane-type air motor exhaust)

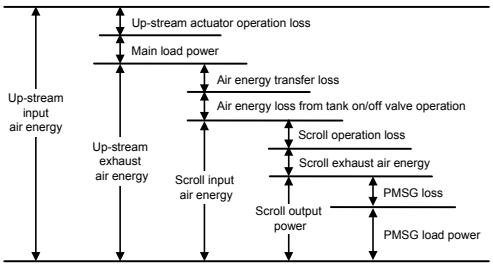

Fig. 12 Energy factors need to be considered for the process of conversion

The pneumatic actuator energy conversion capability can be interpreted as the work extracted from the compressed air while it undergoes a working process from an inlet thermodynamic state to an exhaust thermodynamic state. Thus, it is necessary to find out how much air energy contained in the compressed air inputs to the system and how much it is utilized by the actuator to do the useful work.

The change of air power is below 15% when air temperature shifts 100K from the atmospheric temperature [18]. Thus, if ignoring the effect of temperature change to the air power variation, similarly to the calculation of work done by the air compressor, the air power extracted by the pneumatic actuator ($Q_{actuator}$) can be derived ([16][17]),

$$Q_{actuator}=Q_{airin}-Q_{airout}=\dot{m}_{in}H_{in}-\dot{m}_{out}H_{out} \tag{24}$$

where H_{in} and H_{out} stand for the enthalpy of the air at the inlet port and the outlet port of the actuator respectively. Q_{airin}, Q_{airout} are the system input and output air power individually.

An alternative simplified approach for calculating the air power referred to STP (Standard Temperature and Pressure, with 0^oC at $1atm$) can be expressed by expanding the air enthalpy to the air pressure and temperature ([16][17][18][19]),

$$Q_{air} = \dot{m}RT_{atm}[\ln\frac{P}{P_{atm}} + \frac{k}{k-1}(\frac{T}{T_{atm}} - 1 - \ln\frac{T}{T_{atm}})] \quad (25)$$

where subscript atm is the atmosphere. When the up-stream subsystem is in operation only, the calculation of the up-stream energy efficiency is:

$$\eta_{up} = \frac{Q_{up\_power}}{Q_{actuator}} \quad (26)$$

where Q_{up_power} is the up-stream actuator useful power out, i.e., the main load power. When the overall pneumatic-electrical system is in operation, the definition of the overall system energy efficiency used in the paper is:

$$\eta_{overall} = \frac{Q_{up\_power} + Q_{scroll\_power}}{Q_{airin} - Q_{airout}} = \frac{Q_{up\_power} + Q_{scroll\_power}}{Q_{airin} - Q_{t\_exh} - Q_{s\_exh}} \quad (27)$$

where Q_{scroll_power} is the scroll useful power out, which refers to the 3-phase electrical load. Q_{t_exh} is the air power out through the on/off valve of the air tank. And Q_{s_exh} is the scroll air motor exhaust air power released from the scroll discharging port. In the efficiency analysis, when the vane air motor average speed is kept above 90% of its desired speed, the vane air motor movement is considered to be maintained.

The initial experimental tests to the calculation of the system energy efficiency have been conducted. The pressure limitations of the intermediate air tank are set at $P_{\max} = 2.5\times10^5 Pa$ and $P_{\min} = 2.3\times10^5 Pa$. The experimental results of the energy efficiency for actuator system with and without engaging the exhaust recycling mechanism at different supply pressures have been compared. It is found that, with the same supply pressures, compared to the energy efficiency of the up-stream vane air motor, the overall system energy efficiency can be enhanced about 14%-23%. Thus the pneumatic system energy efficiency is improved. In the tests, it is noticed that the overall pneumatic-electrical system can work properly in a certain range of supply pressures, about from $3.5\times10^5 Pa$ to $6.4\times10^5 Pa$. The working starting point ($3.5\times10^5 Pa$) is the operation point for engaging the recycling scroll-type air motor. And the working ending point ($6.4\times10^5 Pa$) means that it is difficult to maintain the vane-type air motor movement while the supply pressure is higher than the working ending point.

VI. Conclusion

The paper has reported the recent work in development of a novel compressed air energy recovering system. A complete process mathematical model for the system is derived. The simulation study provided fundamental understanding to the system. A laboratory experiment system is built and then tested with an appropriate system control strategy. From the study, it can be concluded that the overall system energy efficiency can be improved. Also, further energy efficiency improvement can be achieved by applying an advanced controller to the system; reducing the pneumatic-electrical system air leakage and restructuring the system structure with more close connections.

References

[1] The Energy Resources Center of the Illinois Industries of the Future, available at: http://www.erc.uic.edu/iof/comp_air.html, viewed 20th February 2010.

[2] M. Horner, "Compressor Control", Engineering & Technology, Vol. 1, No.1, pp24-25, 1998.

[3] G. Belforte, "New developments and new trends in pneumatics", keynote lecture of FLUCOME 2000, the 6th International Symposium on Flow Control, Measurements and Flow Visualization, Canada, 2000.

[4] S. R. Majumdar, *Pneumatic Systems: Principles and Maintenance*, Tata McGraw-Hill, pp.1-33, 1996.

[5] J. Wang, L. Yang, X. Luo, S. Mangan, J.W. Derby, "Mathematical modelling study of scroll air motors and energy efficiency analysis - Part I", *IEEE/ASME Trans. on Mechatronics*, Vol. 16, pp. 112-121, 2011.

[6] T. Yanagisawa, "Performance of an oil-free scroll-type expander", Institution of Mechanical Engineers, Fluid Machinery Group, Institution of Mechanical Engineers, City University, London, 2003.

[7] Y. Chen, N. Halm, E. Groll, J. Braun, "Mathematical modelling of scroll compressors—part I: compression process modeling", *International Journal of Refrigeration*, 25(6), pp731–750, 2002.

[8] J. Wang, U. Kotta, J. Ke, J., "Tracking control of nonlinear pneumatic actuator systems using static state feedback linearisation of input/output map", *Proc. of Estonian Acad. Sci. Phys. Math.*, Vol. 56, No.1, pp47-66, 2007.

[9] X. Luo, J. Wang, L. Shpanin, N. Jia, G. Liu, A. Zinober, "Development of a mathematical model for vane-type air motors with arbitrary N vanes", *The Proceedings of World Congress on Engineering*, 2008.

[10] J. Wang, X. Luo, L. Yang, L. Shpanin, N. Jia, S. Mangan, J.W. Derby, "Mathematical modelling study of scroll air motors and energy efficiency analysis - Part II", *IEEE/ASME Trans. on Mechatronics*, Vol. 16, pp. 122-132, 2011.

[11] A. E. Fitzgerald, C. Kingsley, D. U. Stephen, *Electric Machinery,* fifth edition, Singapore, pp. 254-272, 1992.

[12] Specification of M4-200X dc servomotor, Callan technology, viewed 20th April 2008, available at: http://www.callantechnology.com/callan_technology_products/M4-200X/M4-200X.html.

[13] Handbook of AC synchronous brushless servomotors series EKM, Motor Technology, viewed 18 March 2008, available at: http://www.motec.co.uk/euroServo/documents/es_ekm-hb_mt.pdf.

[14] J. L. Wei, J. Wang, Q. H. Wu, "Development of a multi-segment coal mill model using an evolutionary computation technique", *IEEE Transactions on Energy Conversion*, Vol. 22. pp. 718-727, 2007.

[15] T. Eastop, A. McConkey, *Applied Thermodynamics for Engineering Technologists*, Longman, printed in Singapore, pp12-67, 1993.

[16] M.L. Cai, K. Kawashima, "Power assessment of flowing compressed air", *Journal of Fluids Engineering*, pp402-405, Vol. 128, 2006.

[17] W. L. Kam, *Applied Thermodynamics: Availability Method and Energy Conversion*, Taylor & Francis, pp.10-45, 1995.

[18] M.L. Cai, T. Kagawa, "Energy consumption assessment of pneumatic actuating systems including compressor", *IMechE*, pp381-380, C591/03302001, 2001.

[19] N. Jia, J. Wang, K. Nuttall, J.L. Wei, H.M. Xu, M. Wyszynski, J. Qiao, and M. Richardson, "HCCI engine modelling for real-time implementation and control development", *IEEE/ASME Transactions on Mechatronics*, Vol.12, pp581-589, 2007.